Journal of Power Sources 236 (2013) 230–237

Contents lists available at SciVerse ScienceDirect

Journal of Power Sources

journal homepage: www.elsevier.com/locate/jpowsour

Pseudo-capacitive profile vs. Li-intercalation in Nano-$LiFePO_4$

Yonggang Wang [a], Dan Zhao [c], Renchao Che [b], Yongyao Xia [a,*]

[a] Department of Chemistry and Shanghai Key Laboratory of Molecular Catalysis and Innovative Materials, Institute of New Energy, Fudan University, Shanghai 200433, China
[b] Department of Material Science, Laboratory of Advanced Materials, Fudan University, Shanghai 200433, China
[c] Zhejiang Key Laboratory for Reactive Chemistry on Solid Surfaces, Institute of Physical Chemistry, Zhejiang Normal University, Jinhua, Zhejiang 321004, China

HIGHLIGHTS

- Nano-$LiFePO_4$ achieved a capacity of 80 mAh g^{-1} at a discharge rate of 100 C with limited carbon additive.
- Capacity of $LiFePO_4$ observed above 3.5 V and below 3.4 V is mainly due to the pseudo-capacitive behavior.
- Crystalline-to-amorphous transformations occur on the long-time cycling process of $LiFePO_4$.

ARTICLE INFO

Article history:
Received 11 November 2012
Received in revised form
21 February 2013
Accepted 25 February 2013
Available online 5 March 2013

Keywords:
Lithium iron phosphate
Pseudo-capacitive behavior
Battery behavior
Phase transformation

ABSTRACT

It is well-established that the micro-sized $LiFePO_4$ exhibits very poor rate capability, whereas nano-sized $LiFePO_4$ displays very excellent rate capability. Thereby, kinetic behavior of nano-sized $LiFePO_4$ is attracting wide attention. Herein, it is reported that nano-sized $LiFePO_4$ can realize the fast charge/discharge of 100 C with limited carbon additive. Most importantly, it is discovered that the capacity of $LiFePO_4$ observed above 3.5 V (vs. Li/Li^+) and below 3.4 V (vs. Li/Li^+) is mainly due to the pseudo-capacitive behavior rather than single-phase Li-intercalation, indicating that there is only very small potential difference (100 mV, 3.4–3.5 V) between the single-phase transformation and two-phase equilibrium. Also cycle-life test, combining with TEM observations, demonstrates that the crystalline-to-amorphous transformation in part of nano-$LiFePO_4$ particles during cycling process can result in the change of voltage at the end of charge/discharge.

1. Introduction

Olivine $LiFePO_4$ has been considered as the promising cathode for the large scale lithium-ion batteries used for electric vehicles (EVs) and stationary power sources because of its inherent merits including low toxicity, potential for low cost, long cycle ability and high safety. Owing to these inherent merits mentioned above, it has been attracting significant attention from both the academic and industrial research fields [1]. In 1997, Padhi et al. first reported that olivine $LiFePO_4$ could be used as a cathode material for lithium-ion battery, and showed it could only have a reversible capacity of 110 mAh g^{-1} at a potential of 3.5 V vs. Li/Li^+ when cycled using a very low current density [2]. Accordingly, a lot of efforts have been made to solve this problem by the tailored particle-size or/and the conductivity surface coating [1–8]. Indeed, the rate capability was greatly improved by these approaches, but it still works well limited. Up to 2009, Kang et al. prepared nano-sized $LiFePO_4$ with an ionically conductive lithium phosphate glasses coating layer [8]. The obtained material exhibited an exceptional capacity of 130 mAh g^{-1} even at a discharge rate of 50 C. When the electrode material was prepared with 65% mass of carbon additive, a capacity of more then 100 mAh g^{-1} was achieved at a very fast rate of 200 C, which can be compatible with supercapacitor. This finding clearly demonstrated that fast Li-ion diffusion can occur in the nano-sized $LiFePO_4$. Up to date, such high rate performance (higher than 100 C) is rarely achieved with lower carbon additive.

Recently, many researches shift to study the mechanism of Li-ion storage [9–19], especially in the issues of phase transformation during charge/discharge process, which brings many arguments and new opinions. The thermodynamics and phase diagram of $LiFePO_4$ is now well established. The electrode reaction of $LiFePO_4$ is dominated by the two-phase coexistence of $Li_\alpha FePO_4$ and $Li_{1-\beta}FePO_4$ but with the very narrow single-phase regions ($0 < x < \alpha$ and $1 - \beta < x < 1$) close to the stoichiometric end members of $LiFePO_4$ and $FePO_4$ at room temperature [10,11,20]. According to previous reports [11,13,21,22], Li-ion de-insertion/insertion within the two-phase region is characterized by a very flat

* Corresponding author. Tel./fax: +86 21 51630318.
E-mail address: yyxia@fudan.edu.cn (Y. Xia).

0378-7753/$ – see front matter © 2013 Elsevier B.V. All rights reserved.
http://dx.doi.org/10.1016/j.jpowsour.2013.02.071

potential profile (or a constant two-phase equilibrium potential), whereas Li-ion de-insertion/insertion in the single-phase region displays a slope–potential profile which is above or below the two-phase equilibrium potential. A lot of reports have demonstrated the size-depend nature of the single-phase region with the direct evidence that the capacity contribution from the slope charge/discharge curve clearly increased with the reduction of particle-size [11,13,21,22]. However, it is well-known that the pseudo-capacitive behavior arising from the surface charge storage also displays a slope charge/discharge curve, and its performance scales with its particle-size (or surface areas), specially for the nano-sized materials. Thereby, the size-induced pseudocapacitance variation may misconsidered to determine the single phase behavior in previous reports. Unfortunately, pseudo-capacitive behavior of nano-$LiFePO_4$ is never well investigated during the past years. How to quantificationally distinguish the surface pseudo-capacitive behavior from the single-phase Li-intercalation in the crystalline framework of $LiFePO_4$ is still unclear.

In present work, the as-prepared graphene-supported nano-$LiFePO_4$ delivered a high capacity of 80 mAh g^{-1} even at a charge/discharge rate of 100 C. It is more important that the pseudo-captive behavior of the as-prepared nano-$LiFePO_4$ during charge/discharge process was detailedly investigated in present work. It was discovered that the capacity of $LiFePO_4$ observed above 3.5 V (vs. Li/Li^+) and below 3.4 V (vs. Li/Li^+) is mainly due to the pseudo-capacitive behavior rather than single-phase Li-intercalation. Finally, we found that the capacity contribution from the flat operating voltage gradually reduced over cycling process, and demonstrated that this phenomenon was due to the crystalline-to-amorphous transformation by TEM observation.

2. Experiment

In a typical synthesis of graphene-supported $LiFePO_4$, 12 mmol $FeSO_4{\cdot}7H_2O$,12 mmol H_3PO_4 and 60 mg graphene power were dissolved in 20 ml ethylene glycol under stirring condition. Then, another 15 ml ethylene glycol solution including 32.4 mmol $LiOH{\cdot}H_2O$ was slowly added into the $FeSO_4$–H_3PO_4–ethylene glycol solution with constantly stirring (the molar ratio of $FeSO_4{\cdot}7H_2O$, H_3PO_4 and $LiOH{\cdot}H_2O$ was 1:1:2.7). In the next step, the mixture was sealed into a 40 ml autoclave and heated at 180 °C for 10 h. After solvothermal treatment, the reaction mixture was separated by filtration. The solid product was subsequently washed several times with deionized water, and then dried in air at 60 °C for 12 h. Afterward, the as-prepared reaction mixture ($LiFePO_4$ + graphene) was mixed with 11 wt.% sucrose as carbon source (ratio of $LiFePO_4$:C is about 1:0.05, w/w). Finally, the mixture ($LiFePO_4$ + graphene + sugar) was first calinated in Ar atmosphere at 200 °C for 0.5 h, and then heated to 550 °C for 2.5 h to obtain the finial product of graphene-supported $LiFePO_4$.

Power X-ray diffraction (XRD) of the prepared materials was recorded on Bruker D8 Advance Diffractometer using Cu K radiation. The morphologies of the sample were characterized with transmission electron microscope (TEM, Joel JEM2010). Nitrogen sorption isotherms were measured at 77 K after being degassed at 300 °C for at least 3 h (Quadrasorb *SI* Automated Surface Area and Pore Size Analyzer). Specific surface area of the sample were derived using the multipoint Braunauer–Emmett–Teller (BET) method. The analysis for elementary distribution was performed on Energy Dispersive X-ray Detector (EDX, Superscan SSX-550).

Half cells (CR2016 coin-type) were fabricated to investigate the electrochemical behavior of graphene-supported $LiFePO_4$. The as-prepared $LiFePO_4$/graphene composite (80 wt.%) was mixed with 15 wt.% carbon black and 5 wt.% polyvinylidene fluoride (PVDF), using *n*-methylpyrrolidone (NMP) as the solvent, and then was spread on aluminum foil current collect to form a working electrode. Li metal foil was used as the counter and reference electrode, and 1 $LiPF_6$ dissolved in 1:1 v/v mixture of ethylene carbonate/diethyl carbonate (EC/DEC) was employed as the electrolyte. The mass loading of graphene-supported $LiFePO_4$ in working electrode is 2.60 mg cm^{-2}. Solartron Instrument Model 1287 electrochemical interface and 1255B frequency response analyzer were employed for electrochemical impedance spectroscopic (EIS) measurements, potentiostatic intermittent titration technique (PITT) measurements as well as charge/discharge tests at different currents. Prior to each EIS measurement, the cell was charged/or discharged to a special potential and hold at this potential. Each subsequent potential step was finished after the residual (background) current was less then 1/300 C. Then, EIS measurement was performed at this potential in the frequency range 10^6–0.01 Hz with AC signal amplitude of 5 mV. For PITT measurement, the cell potential is steeped by special increments from 2.5 V to 4.3 V. Each individual titration (at a potential step) is terminated when the current decreased to 1/200 C. Charge/discharge cycle was performed 2.0 V and 4.3 V using a LAND CT2001A Battery Cycler (Wuhan, China). Detail information about the cycling test was given in supporting information.

3. Results and discussion

3.1. Pseudo-capacitive profile vs. Li-intercalation in nano-$LiFePO_4$

We used layered graphene as loading medium and employed carbon coating technology to prepare carbon modified nano-$LiFePO_4$. Fig. 1a–c depicts the different magnification transmission electron microscopy (TEM) image of the prepared graphene-supported nano-$LiFePO_4$. TEM image in Fig. 1a shows that $LiFePO_4$ nanoparticles with a typical size of ~50 nm in diameter are uniformly loaded on the surface of layered graphene. Besides it, many $LiFePO_4$ nanoparticles were wrapped in the flexible and ultrathin graphene shells (see Fig. 1b). The amount of graphene in the prepared composite is estimated as about 5% by calculating the weight difference between graphene precursor and the final product of $LiFePO_4$/graphene composite. The high resolution TEM image shown in Fig. 1c clearly reveals that each primary crystallite of $LiFePO_4$ is coated by a thin carbon layer which arises from carbonization of the sugar precursor (Detail information for the formation of carbon coating layer is given in Experiment section). The wt.% of the thin carbon coating layer is very low, and can be neglected. The special BET surface of the prepared graphene-supported nano-$LiFePO_4$ is 29.6 m^2 g^{-1}. The X-ray diffraction (XRD) pattern of prepared composite is shown in Fig. 1d. All the diffraction peaks can be indexed on the basis of an olivine structure of $LiFePO_4$.

As mentioned in introduction, many researches reported the shape of charge/discharge curves depends on the size of $LiFePO_4$ particle, especially at the beginning/end of charge/discharge, which are typically considered to be associated with the phase composition [11,13,21,22]. However, we speculated it is mainly results from the pseudo-capacitive behavior which is produced from the fast, reversible Faradaic reaction occurring at or near a solid electrode surface [23–28]. Pseudo-capacitive behavior generally shows the successive multiple surface redox reactions within a wide potential window, and thus displays slope potential (or voltage) profile on charge/discharge process [27]. Owing to the character of surface energy storage, pseudo-capacitive behavior is also typically size-dependent. In order to distinguish the pseudo-capacitive behavior from the single-phase Li-intercalation, electrochemical impedance spectroscopic (EIS) analysis of the graphene-supported nano-$LiFePO_4$ at different charge/discharge depth (or potential)

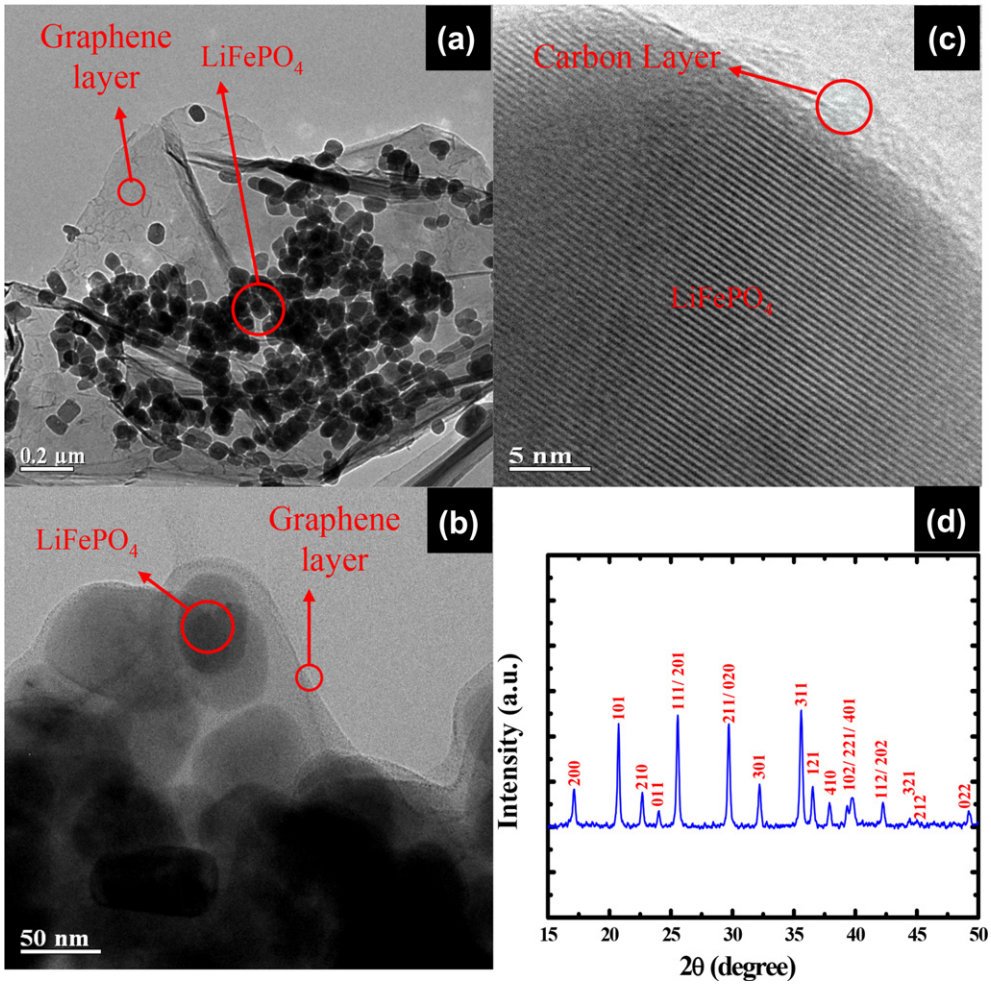

Fig. 1. TEM images (a, b, c) and XRD pattern (d) of graphene-supported nano-$LiFePO_4$.

was conducted on charge/discharge process. Impedance phase angle data collected at selected charge/discharge depths are shown in Fig. 2. The impedance phase angles at low frequency ranges can be clearly divided into groups (see Fig. 2): One is larger than 45° indicating the electrochemical reaction without diffusion limitation; another is close to (or lower than) 45° indicating the electrochemical reaction with diffusion limitation. When the electrode was charged in charge-potential region from 2.0 to 3.4 V (2.0 < 3.4 V), impedance phase angles close to −90° over a wide frequency range are detected at low frequency, indicating that the capacity contribution within the potential window from 2.0 to 3.4 V arises from pseudo-capacitive behavior (or surface redox reaction). This is because that the impedance phase angle close to 90° is the typical character of capacitive behavior [23–25,28], indicating that the charge storage behavior is not controlled by diffusion process. When the working electrode is further charged to 3.4 V (vs. Li/Li^+), it can observed that the impedance phase angle at low frequency is reduced to −45°, which indicates the character of diffusion limitation [23–25]. This phenomenon is kept in the charge-potential range from 3.4 to 3.5 V (3.4 ≤ 3.5 V, vs. Li/Li^+), indicating typical battery behavior (see Fig. 2a and c). At the end of charge process from 3.5 V to 4.3 V (3.5 < 4.3 V vs. Li/Li^+), the impedance phase angles at 0.01 Hz appear again close to −90°, suggesting typical capacitive behavior. Similar with charge process, the frequency response of impedance phase angle at low frequency range in the discharge potential window from 4.3 to 3.5 V and from 3.39 to 2.0 V appears approximating to −90° (see Fig. 2b and c). While impedance phase angles at low frequency within a narrow potential window from 3.5 V to 3.39 V (vs. Li/Li^+) are close to or lower than −45°. The results from EIS investigation clearly demonstrate that the single-phase and two-phase Li-intercalations occur in a very narrow potential range between about 3.4 V and 3.5 V (vs. Li/Li^+). This result is well agree with Ceder et al.'s very recent calculation result that only minimal over-potential is required to enable the single-phase transformation at room temperature [17]. At this stage, we can conclude that the capacity observed above 3.5 V (vs. Li/Li^+) and below 3.4 V (vs. Li/Li^+) is mainly due to the surface pseudo-capacitive behavior, rather than the bulk single-phase Li-intercalation. It should be noted that the double layered electrochemical capacitance from the ions (charge) adsorption/desorption on the graphene-substrate can be neglected (see Fig. S1 for detail).

In order to further determine whether or not both the single-phase and two-phase Li-intercalations take place in a very narrow potential range (about 3.4–3.5 V, vs. Li/Li^+), the potentiostatic intermittent titration technique (PITT) technology was employed on charge process. For PITT measurement, the cell potential is steeped by special increments from 2.5 V to 4.3 V. Each individual titration (at a potential step) is terminated when the current decreased to 1/200 C. 100 mV potential steps were applied for PITT measurement in the pseudo-capacitive behavior region (from 2.5 to 3.4 V and from 3.5 to 4.3 V, vs. Li/Li^+), and 10 mV potential steps were employed in the battery behavior region from

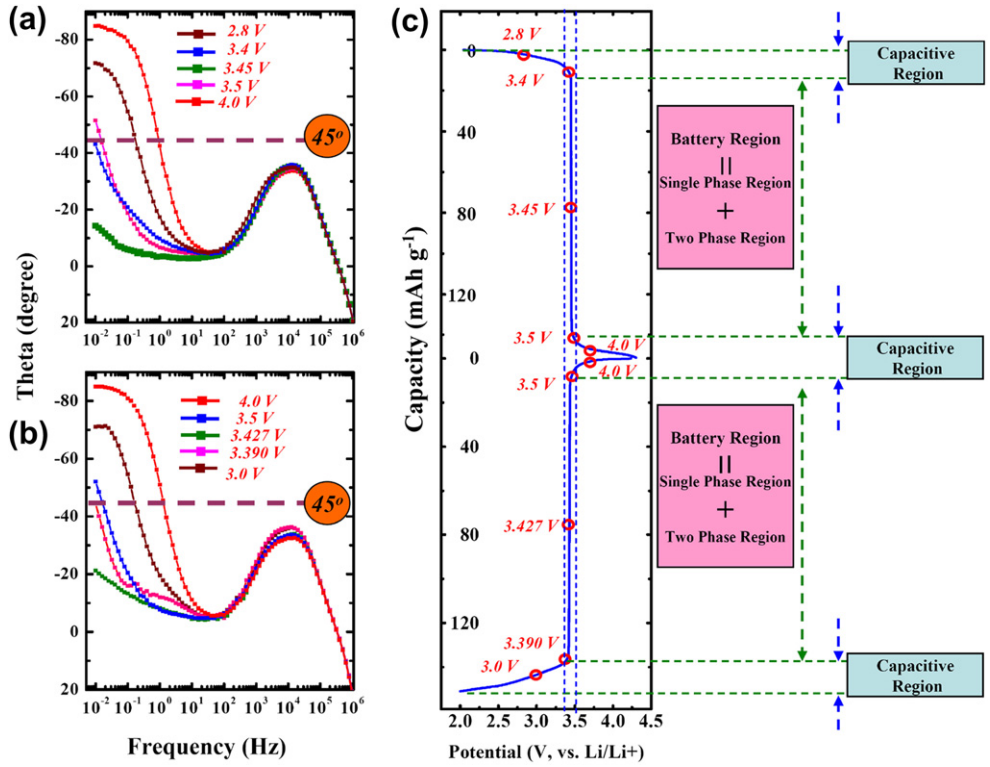

Fig. 2. Impedance phase angle vs. frequency for the graphene-supported $LiFePO_4$ at different charge depths (a) and discharge depths (b). The corresponding charge/discharge at a current density of 1/20 C is also given in (c).

3.4 to 3.5 V (vs. Li/Li^+). Fig. 3a and b gives the PITT potential steps and corresponding current relaxation curves. As shown in Fig. 3b, even with the potential steps of 100 mV, the current relaxation process in the pseudo-capacitive region only needs very short time. Although 10 mV potential steps were employed in the battery behavior region from 3.4 to 3.5 V, the current relaxation still keeps much longer time than that in pseudo-capacitive region. As shown in Fig. 3a and c, the potential profile is pretty flat in the middle of battery behavior region, which is owing to the two-phase coexistence. Furthermore, the current relaxation behavior (I vs. t) has

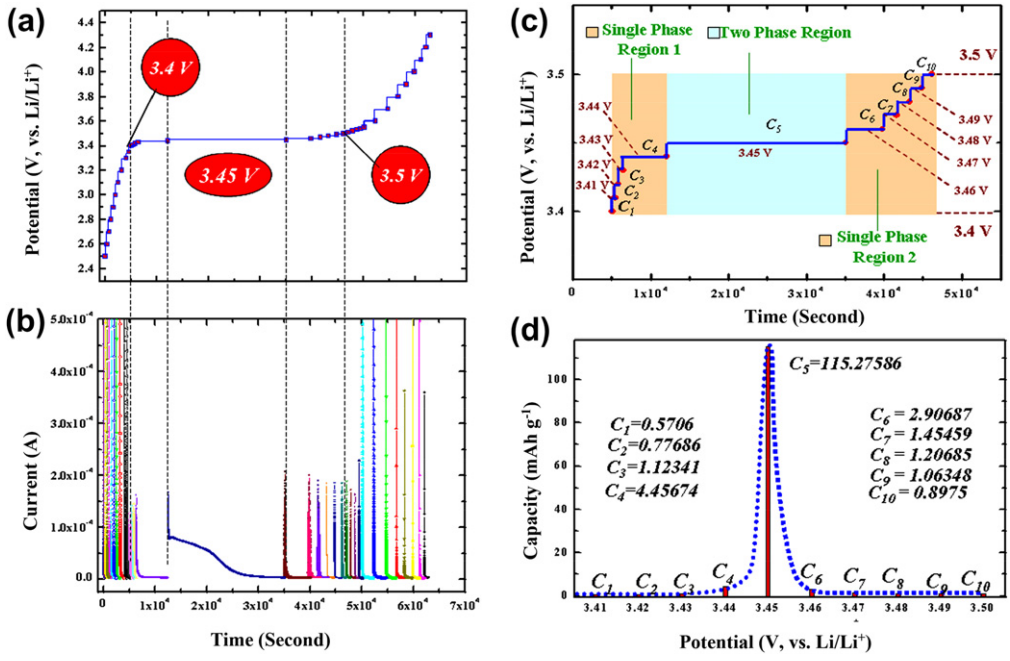

Fig. 3. PITT measurements upon charge process (a) and the corresponding current relaxation curves (b); the enlargement of PITT measurements in the potential window from 3.4 to 3.5 V (c) and the calculated capacity on each potential step (d).

markedly different behavior and characteristic times in the single phase region vs. the two-phase region (see Fig. 3b and c). In two-phase range, the current relaxation behavior (or the curve of I vs. t) has an obvious plateau, which may be the character of phase-transition-limited process [29]. However, in the single-phase range, curves of current relaxation (I vs. t) don't have this phenomenon, and display the character of diffusion-limited relaxation [29]. The capacity contribution on each individual titration (at a potential step of 10 mV) in the battery behavior region was calculated from it corresponding current relaxation curve (I vs. t) and the results were summarized in Fig. 3d. As shown in Fig. 3c and d, the capacity contribution from the two-phase coexistence region is 115.28 mAh g^{-1} (C_5). The capacity contributions out of the two-phase coexistence region are 6.92 mAh g^{-1} ($=C_1 + C_2 + C_3 + C_4$) and 7.51 mAh g^{-1} ($=C_6 + C_7 + C_8 + C_9 + C_{10}$), respectively (see Fig. 3c and d). The total capacity contribution from pure battery behavior (single-phase Li-intercalation + two-phase Li-intercalation) should be 129.43 mAh g^{-1} ($=6.92 + 115.28 + 7.51$) which is well agreed with the charge curve shown in Fig. 2. It is worth noting that a very small amount of capacity may arise from the mixture of capacitive behavior and battery behavior, which is not included in the capacity (129.43 mAh g^{-1}) from pure battery behavior. Accordingly, the capacity from capacitive behavior should be close to (or/and less than) ~20 mAh g^{-1} (=150–129.43 mAh g^{-1}). In previous report about $LiFePO_4$ [22], it has been reported that the surface portion of the particle abruptly increases when the size is smaller than 100 nm. A simple estimation, based on a spherical particle, provides surface (one unit cell) portions of ~4, 7, and 17% for particles with 100, 50, and 20 nm diameters, respectively [22]. In our manuscript, the particle-size of $LiFePO_4$ is about 50 nm, indicating a surface portion of ~7%. The calculated capacity arising from the surface redox reaction should be ~12 mAh g^{-1} ($=7\% \times 170$ mAh g^{-1}). In addition, the $LiFePO_4$/carbon composite also displays electrochemical double layered capacitance which can be estimated by 20 mF cm^{-2} [30]. In view of the surface area of the composite (29.6 m^2 g^{-1}), the calculated capacitance should be 5.8 F g^{-1}, and can be converted into the capacity of 3.7 mAh g^{-1} (The electrode is cycled in the voltage window from 2.0 V to 4.3 V). The calculated capacity from capacitive behavior is 15.7 mAh g^{-1} ($=12 + 3.7$ mAh g^{-1}), and is close to ~20 mAh g^{-1}. Furthermore, it is a common phenomenon that the open circuit voltage (OCV) of $LiFePO_4$/Li cell changes after full charge or discharge. This phenomenon may be attributed to that the self-discharge of surface pseudo-capacitive behavior is much more serious than that of battery behavior. It is well known that the self-discharge of supercapacitors is much more obvious than that of batteries.

3.2. Fast charge/discharge of graphene-supported nano-$LiFePO_4$

The electrochemical profile of the graphene-supported nano-$LiFePO_4$ was evaluated. The mass loading of graphene-supported nano-$LiFePO_4$ in working electrode is 2.60 mg cm^{-2}, in corresponding to 2.44 mg cm^{-2} of pure active material ($LiFePO_4$). The total wt% of carbon additive (carbon black + graphene supporter) is 19% (see electrode preparation in Experimental section for details). Fig. 4 gives the charge/discharge curves of graphene-supported nano-$LiFePO_4$ within the voltage window from 2.0 V–4.3 V (vs. Li/Li^+) at different current densities. As shown in Fig. 4, the prepared graphene-supported $LiFePO_4$ exhibits a reversible charge/discharge capacity of 152 mAh g^{-1} at a charge/discharge current density of 0.5 A g^{-1} (about 3 C). When the current density is increased to 10 A g^{-1} (about 65 C), the prepared graphene-supported nano-$LiFePO_4$ displays a capacity of 110 mAh g^{-1}. Even at much higher rate (16 A g^{-1} or 100 C), corresponding to finishing

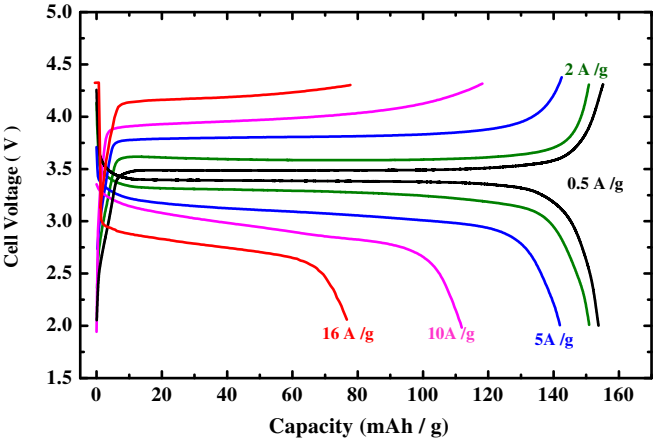

Fig. 4. Charge/discharge curves of graphene-supported $LiFePO_4$ at different current densities, varying from 0.5, 2, 5, 10 A g^{-1} to 16 A g^{-1}.

the full charge or discharge in 36 s, the prepared material still keeps a capacity of ~80 mAh g^{-1}. The result shown in Fig. 4 is consistent with the excellent rate performance reported by Kang et al. [8]. The excellent rate capability of the graphene-supported nano-$LiFePO_4$ was confirmed by cyclic voltammetry (CV) investigations (see Fig. S2 for detail).

We believed that the excellent rate capability of the graphene-supported nano-$LiFePO_4$ is due to both fast electronic and ionic transportation path. Firstly, the novel structure of designed graphene-supported nano-$LiFePO_4$ provides fast electronic transportation path: The low mass loading (2.44 mg cm^{-2}) of active material ($LiFePO_4$) effectively shorten electron transfer length from current collector to composite active material. Graphene supporter

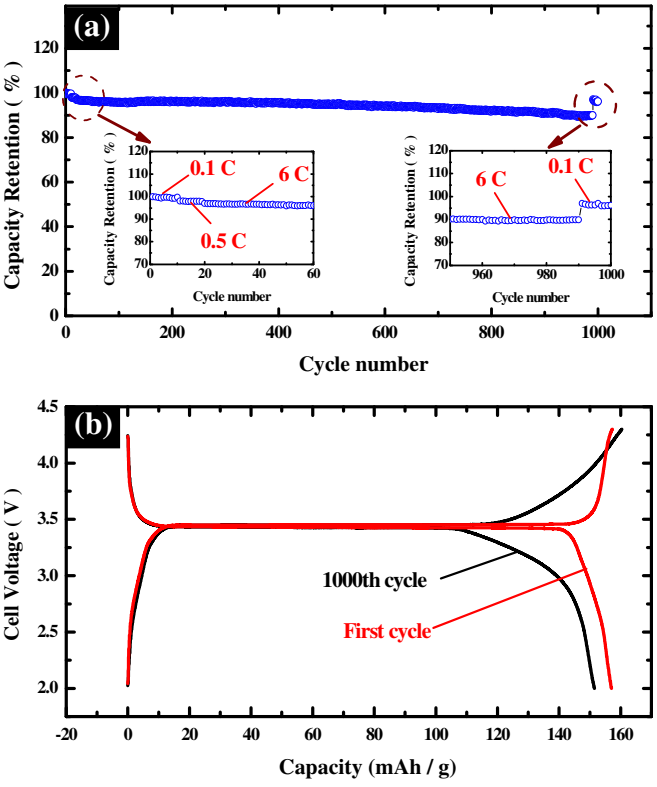

Fig. 5. Cycle performance of graphene-supported $LiFePO_4$ (a) and the charge/discharge curves at different cycles (b).

ensures the deliver of electrons from current collector to each $LiFePO_4$ particle. The thin carbon coating layer facilities the deliver of electron around out surface of $LiFePO_4$ whole nanoparticles; Secondary, it is well-known that Li-ions can only be inserted into the framework of $LiFePO_4$ on (010) face, suggesting that the reaction can only occur on the selected spots where the Li^+ is supported. Kang et al. considered that the high rate capability is due to that the amorphous nature of the coating ($Li_4P_2O_7$) removes the anisotropy of the surface properties and enhances delivery of Li^+ to the (010) facet of $LiFePO_4$ where it can be inserted [8]. In our case, we expected that the pseudo-capacitive behavior (surface redox reaction: Surface-$Fe^{2+} + Li^+ + e^- \rightarrow$ Surface-$Fe^{2+}||Li^+$) results in Li-ions quick congregation on the surface at all directions without diffusion limitation. It should be noted that the fast Li-diffusion in the thin low crystalline coating layer (existing defects) has confirmed by many research groups in experimental and theoretical calculation [31–33]. Finally, the high rate capability of the graphene-supported nano-$LiFePO_4$ is also due to both the short Li-ion diffusion length in the crystalline framework (50 nm particle) and size-dependent diffusion rate [34] (see Fig. S3).

3.3. Crystalline-to-amorphous transformation on cycling process

The cycling behavior of the graphene-supported nano-$LiFePO_4$ was further characterized by continuous charge/discharge cycle within the voltage window from 2.0 to 4.3 V (Detail information about the cycle test is given in Fig. S4). As expected, the as-prepared $LiFePO_4$/graphene composite exhibits very excellent capacity retention with less than 5% discharge capacity loss over 1000 cycles (in Fig. 5a). Fig. 5b gives the charge–discharge curves of the $LiFePO_4$/graphene composite at initial cycle and 1000th cycle. It is most interesting that although the capacity loss is almost negligible between the first and 1000th cycles in potential window from 2.0 to 4.3 V, the shape curve at the end of charge/discharge are significantly changed, becoming a sloping upon cycling. However, this phenomenon does not occur at the beginning of charge/discharge. Apparently, this phenomenon cannot solely attribute to the increase in pseudocapacitance. The reason for this phenomenon should be a new and interesting problem. Especially, in Wang et al.'s previous investigation [7], nano-$LiFePO_4$ was investigated with three-electrode experiment, where metallic Li is used as counter electrode and reference electrode. Over 1100 cycles, the voltage–capacity profile of electrode displays the same phenomenon [7]. After the cycled Li metal electrode is replaced by a fresh one, the phenomenon still can be observed clearly (Fig. S5).

After cycle test, we employed TEM technology to observed different cycled $LiFePO_4$ particles. Herein, we only randomly choose several typical cycled $LiFePO_4$ particles (Particle-A, B, C and D) and give their corresponding high resolution TEM images in Fig. 6a–d. As shown in Fig. 6a, particle-A still exhibits crystalline character after 1000 charge/discharge cycles. However, the TEM image shown in Fig. 6b indicates that particle-B displays the amorphous character. In Fig. 6c, partial amorphous region in particle-C can be clearly observed. The selected-area electron diffraction patterns (SAED) suggests that the out surface of particle-D is amorphous, whereas its internal region is sill crystalline (see Fig. 6d). All of

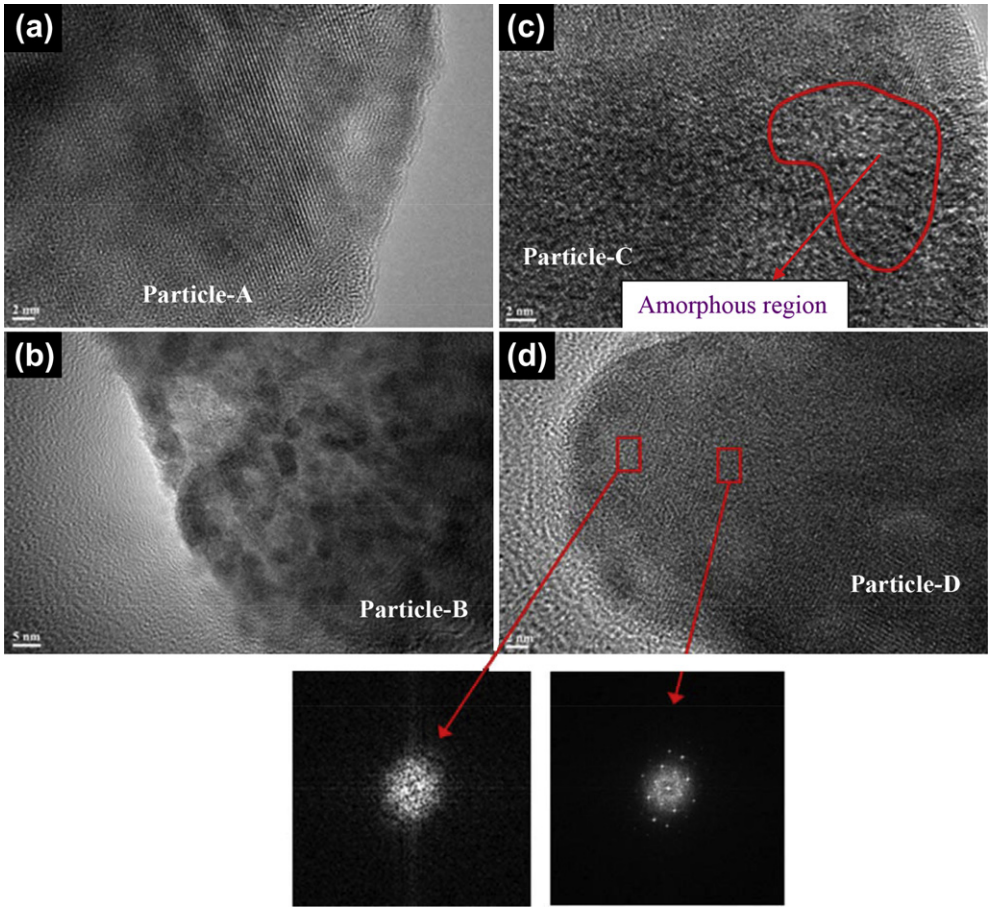

Fig. 6. TEM images of cycled $LiFePO_4$ particles. Herein, we randomly choose several typical cycled $LiFePO_4$ particles (Particle-A, B, C and D) and give their corresponding high solution TEM images (Fig. 6a–d).

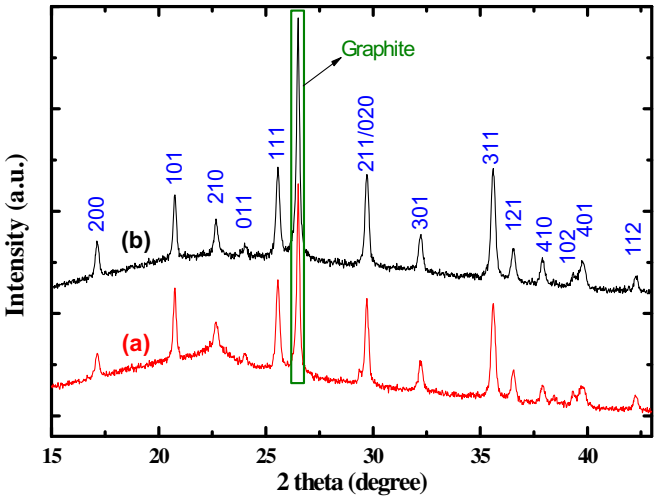

Fig. 7. XRD patterns of the cycled $LiFePO_4$ electrode (a) and fresh $LiFePO_4$ electrode (b).

these results indicate the repeated charge/discharge has various impacts on different $LiFePO_4$ particles because the size of $LiFePO_4$ particles is not absolutely equal. According to Tang et al. [35] recent calculation, crystalline-to-amorphous transformation may be preferred in smaller $LiFePO_4$ particles. [Their calculation indicates that the electrical overpotential applied to $LiFePO_4$ is a fundamental parameter that influences the kinetic competition between crystalline-to-crystalline and crystalline-to-amorphous transformations, and predicts that nano-$LiFePO_4$ should take the crystalline-to-amorphous transformation because decreasing particle size expands the overpotential region in which amorphization is preferred (Please see Ref. [35] for detail)]. Furthermore, various $LiFePO_4$ particles also have different local conditions, such as the contact with carbon and the wettability of electrolyte.

In Fig. 7, the XRD patterns of fresh $LiFePO_4$ electrode and the cycled $LiFePO_4$ electrode are compared. The character peak of the graphite powder, which is used as a referee, can be observed at 2 theta = 26.5° in Fig. 7. Comparing the line (a) and line (b) of Fig. 7, it can be observed that the fresh $LiFePO_4$ and cycled $LiFePO_4$ have same character peaks. However, their peaks intensities are different. For example, the peaks intensities of cycled $LiFePO_4$ at 17° (200 face), 22.6° (210 face), 24.0° (011 face), 32.2° (301 face) and 39.7° (401 face) are lower than that of fresh $LiFePO_4$. It can be assumed the reduction of peak intensity may arise from the partially amorphization of $LiFePO_4$ particles which has been demonstrated in Fig. 6. On the other hand, our further investigation excludes the possibility of Fe^{3+} dissolution (Please see Fig. S6, S7 for detail).

As mentioned above, the character of cycled composite electrode can be briefly summarized as: it includes some amorphous nano-$LiFePO_4$ particles and other crystalline nano-$LiFePO_4$ particles. We believe that the generation of nano-amorphous $LiFePO_4$ particles results in the change of charge/discharge curve. The arrangement of atoms in these amorphous nano-$LiFePO_4$ particles (see Fig. 6b–d) is high disordered and that the structure disorder is a more likely cause for the sloping voltage profile. In order to clarify this point, we also prepared another kind of nano-$LiFePO_4$ through the same solvothermal synthesis at 180 °C without following heat treatment process (Here, it is called as "low temperature prepared $LiFePO_4$"). It is undoubted that the low temperature prepared $LiFePO_4$ should be obvious disordered, compared with these $LiFePO_4$ synthesized with heat treatment at high temperature. In Fig. 8a, we give the charge/discharge profile at a rate of 1/20 C of the low temperature prepared nano-$LiFePO_4$. It can be detected in Fig. 8a that the low temperature prepared nano-$LiFePO_4$ displays a charge/discharge capacity of about 120 mAh g^{-1} with a sloping voltage profile. Furthermore, the most of capacity contribution is higher (in charge) or lower (in discharge) than the equilibrium potential. According to this result, the interesting phenomenon about the voltage variation can be explained by Fig. 8b. As shown in Fig. 8b, the total discharge curve at 1000th cycle can be summarized as: I) the slope curve at the beginning of discharge, in which the discharge capacity mainly arises from the capacitive behavior; II) the flat curve at the middle of discharge, where the capacity is mainly contributed by the battery behavior of these crystalline nano-$LiFePO_4$ particles; III) the slope curve at the end of discharge, where the capacity is mainly produced by the battery behavior of these amorphous nano-$LiFePO_4$ particles. EIS measurement was also employed to investigate the cycled $LiFePO_4$ electrode at selected discharge depths after 1000 cycles, and the typical result is given in Fig. 9. As shown in Fig. 9, impedance angle at low frequency is lower than 45°, which indicates the character of diffusion limitation (or a battery behavior = Li-intercalation). This demonstrates that the slope curve at the end of discharge has been converted into battery behavior (=Li-intercalation). The results from Figs. 6 and 9 and Fig. S8 demonstrate that the crystalline-to-amorphous transformation in part of nano-$LiFePO_4$ particles during cycling can result in the change of voltage at the end of charge/discharge. Although there is negligible capacity fading on the long

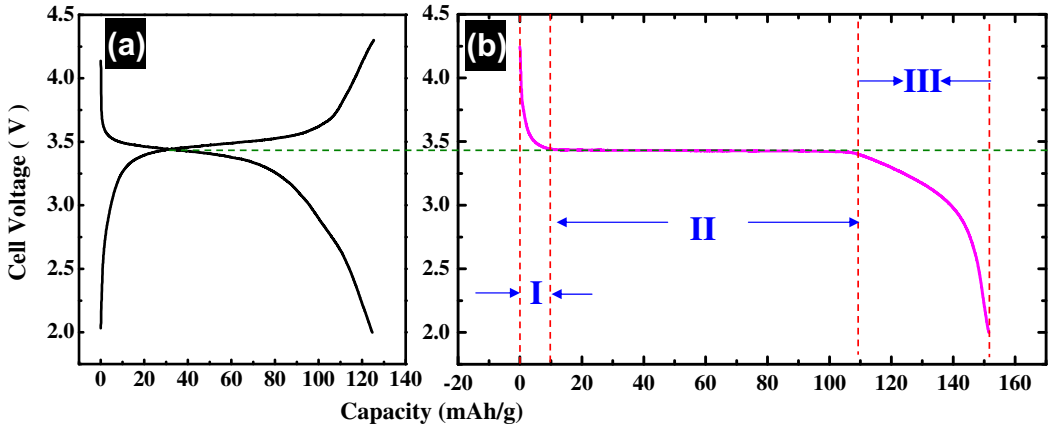

Fig. 8. Charge/discharge curve of low temperature prepared $LiFePO_4$ (a) and the explanation about discharge curve variation after 1000 cycle (b): I) capacity mainly arises from the pseudo-capacitive behavior; II) capacity is mainly contributed by the battery behavior of these crystalline nano-$LiFePO_4$ particles; III) capacity is mainly produced by the battery behavior of these amorphous nano-$LiFePO_4$ particles.

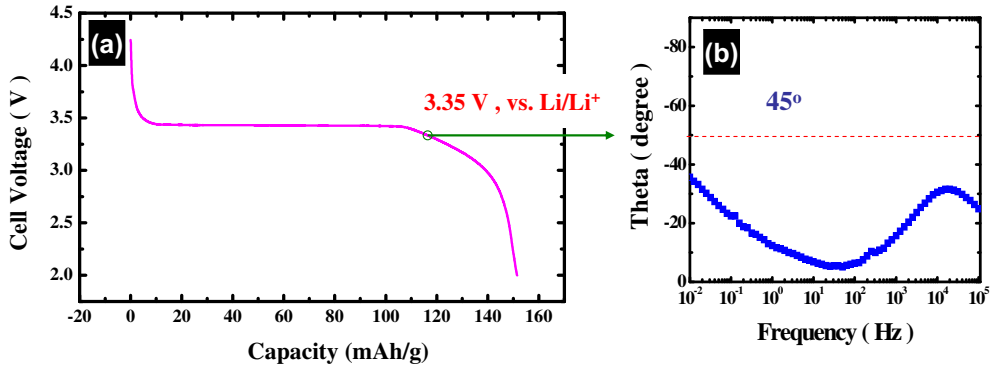

Fig. 9. EIS measurement at selected discharge depths of 3.35 V after the 1000 cycles.

cycling process of nano-$LiFePO_4$, the energy loss arising from the reduction of operating potential is still obvious.

4. Conclusion

By employing various electrochemical analysis technologies, we discovered that the capacity of $LiFePO_4$ observed above 3.5 V (vs. Li/Li^+) and below 3.4 V (vs. Li/Li^+) is mainly due to the pseudo-capacitive behavior, rather than single-phase Li-intercalation. This result demonstrates that both single-phase and two-phase Li-intercalations occur within a very narrow potential window, indicating that only minimal overpotential is required to enable the single-phase transformation at room temperature. Finally, it is found that although $LiFePO_4$ has excellent capacity retention, its electrochemical behavior varies over the charge/discharge cycles, which break through the conventional knowledge that $LiFePO_4$ has very excellent cycle life. The achieved results indicate that the crystalline-to-amorphous phase transition on Li-ion de-insertion/insertion process may result in the amorphization of a part of $LiFePO_4$ particles which lead to obvious energy loss over cycling process.

Acknowledgments

We acknowledge funding support from the National Natural Science Foundation of China (21103025, 20925312), the State Key Basic Research Program of PRC (2011CB935903), and Shanghai Science & Technology Committee (11DZ1100207, 08DZ2270500).

Appendix A. Supplementary data

Supplementary data related to this article can be found at http://dx.doi.org/10.1016/j.jpowsour.2013.02.071.

References

[1] B.L. Ellis, K.T. Lee, L.F. Nazar, Chem. Mater. 22 (2010) 691.
[2] A.K. Padhi, K.S. Nanjundaswamy, J.B. Goodenough, J. Electrochem. Soc. 144 (1997) 1188.
[3] A. Yamada, S.C. Chung, K. Hinokuma, J. Electrochem. Soc. 148 (2001) A224.
[4] H. Huang, S.-C. Yin, L.F. Nazar, Electrochem. Solid State Lett. 4 (2001) A170.
[5] Z.H. Chen, J.R. Dahn, J. Electrochem. Soc. 149 (2002) A1184.
[6] S.Y. Chung, J.T. Bloking, Y.M. Chiang, Nat. Mater. 1 (2002) 123.
[7] Y.G. Wang, Y.R. Wang, E.J. Hosono, K.X. Wang, H.S. Zhou, Angew. Chem. Int. Ed. 47 (2008) 7461.
[8] B. Kang, G. Ceder, Nature 458 (2009) 190.
[9] P.S. Herle, B. Ellis, N. Coombs, L.F. Nazar, Nat. Mater. 3 (2004) 147.
[10] C. Delacourt, P. Poizot, J.M. Tarascon, C. Masquelier, Nat. Mater. 4 (2005) 254.
[11] A. Yamada, H. Koizumi, S.I. Nishimura, N. Sonoyama, R. Kanno, M. Yonemura, T. Nakamura, Y. Kobayashi, Nat. Mater. 5 (2006) 357.
[12] B.L. Ellis, W.R.M. Makahnouk, Y. Makimura, K. Toghill, L.F. Nazar, Nat. Mater. 6 (2007) 749.
[13] P. Gibot, M. Casas-Cabanas, L. Laffont, S. Levasseur, P. Carlach, S. Hamelet, J.M. Tarascon, C. Masquelier, Nat. Mater. 7 (2008) 741.
[14] S. Nishimura, G. Kobayashi, K. Ohoyama, R. Kanno, M. Yashima, A. Yamada, Nat. Mater. 7 (2008) 707.
[15] C. Delmas, M. Maccario, L. Croguennec, F. Le Cras, F. Weill, Nat. Mater. 7 (2008) 665.
[16] W. Dreyer, J. Jamnik, C. Guhlke, R. Huth, J. Moskon, M. Gaberscek, Nat. Mater. 9 (2010) 448.
[17] R. Malik, F. Zhou, G. Ceder, Nat. Mater. 10 (2011) 587.
[18] P. Bai, D.A. Cogswell, M.Z. Bazant, Nano Lett. 11 (2011) 4890.
[19] Y.G. Wang, P. He, H.S. Zhou, Energy Environ. Sci. 4 (2011) 805.
[20] F. Zhou, T. Maxisch, G. Ceder, Phys. Rev. Lett. 97 (2006) 155704-1–155704-4.
[21] N. Meethong, H.Y.S. Huang, W.C. Carter, Y.M. Chiang, Electrochem. Solid State Lett. 10 (2007) A134.
[22] G. Kobayashi, S. Nishimura, M.S. Park, R. Kanno, M. Yashima, T. Ida, A. Yamada, Adv. Funct. Mater. 19 (2009) 395.
[23] B.E. Conway, Electrochemical Supercapacitors: Scientific Fundamentals and Technological Applications, Kluwer Academic/Plenum Publishers, New York, 1999.
[24] B.E. Conway, J. Electrochem. Soc. 138 (1991) 1539.
[25] R. Kötz, M. Carlen, Electrochim. Acta 45 (2000) 2483.
[26] Y.G. Wang, H.Q. Li, Y.Y. Xia, Adv. Mater. 18 (2006) 2619.
[27] P. Simon, Y. Gogosti, Nat. Mater. 7 (2008) 845.
[28] J.R. Miller, R.A. Out, B.C. Holloway, Science 329 (2010) 1637.
[29] N. Meethong, Y.H. Kao, W.C. Carter, Y.M. Chiang, Chem. Mater. 22 (2010) 1088.
[30] L. Cao, M. Lu, H.L. Li, J. Electrochem. Soc. 152 (2005) A871.
[31] L. Cheng, X.L. Li, H.J. Liu, H.M. Xiong, P.W. Zhang, Y.Y. Xia, J. Electrochem. Soc. 154 (2007) A692.
[32] J. Suzuki, M. Yoshida, C. Nakahara, K. Sekine, M. Kikuchi, T. Takamura, Electrochem. Solid State Lett. 4 (2001) A1.
[33] Z.H. Xiong, S.Q. Shi, C.Y. Ouyang, M.S. Lei, L.Y. Hu, Y.H. Ji, Z.X. Wang, L.Q. Chen, Phys. Lett. A 337 (2005) 247.
[34] R. Malik, D. Burch, M. Bazant, G. Ceder, Nano Lett. 10 (2010) 4123.
[35] M. Tang, W.C. Carter, J.F. Belak, Y.M. Chiang, Electrochim. Acta 25 (2010) 969.